System for MR Image–guided Prostate Interventions: Canine Study[1]

Robert C. Susil, BS
Axel Krieger, MS
J. Andrew Derbyshire, PhD
Attila Tanacs, BS
Louis L. Whitcomb, PhD
Gabor Fichtinger, PhD
Ergin Atalar, PhD

Index terms:
Magnetic resonance (MR), experimental studies, 844.121411, 844.121412, 844.121416, 844.12143, 844.12149
Magnetic resonance (MR), guidance, 844.121411, 844.121412, 844.121416, 844.12143, 844.12149
Prostate neoplasms
Prostate neoplasms, MR, 844.121411, 844.121412, 844.121416, 844.12143, 844.12149
Prostate neoplasms, therapeutic radiology, 844.12149

Published online
10.1148/radiol.2283020911
Radiology 2003; 228:886–894

Abbreviations:
GRE = gradient echo
SE = spin echo

[1] From the Departments of Biomedical Engineering (R.C.S., E.A.), Mechanical Engineering (A.K., L.L.W.), Computer Science (A.T., G.F.), and Radiology (E.A.), Johns Hopkins University School of Medicine, 720 Rutland Ave, Traylor Bldg 330, Baltimore, MD 21205; Laboratory of Cardiac Energetics, National Institutes of Health, Bethesda, Md (J.A.D.); and Department of Electrical Engineering, Bilkent University, Ankara, Turkey (E.A.). Received July 31, 2002; revision requested September 30; revision received October 28; accepted December 10. Supported in part by NIH grants R01 HL57483 and R01 HL61672. Additional support from NSF grant ERC 9731478 and U.S. Army grant PC 10029. R.C.S. supported by an NIH training grant. **Address correspondence to** E.A. (e-mail: *eatalar@mri.jhu.edu).*

Author contributions:
Guarantors of integrity of entire study, R.C.S., A.K., G.F., E.A.; study concepts, R.C.S., A.K., L.L.W., G.F., E.A.; study design, all authors; literature research, R.C.S.; experimental studies, R.C.S., A.K., A.T., G.F., E.A.; data acquisition, R.C.S., A.K., A.T., G.F., E.A.; data analysis/interpretation, R.C.S., A.K.; manuscript preparation, R.C.S.; manuscript definition of intellectual content, R.C.S., A.K., L.L.W., G.F., E.A.; manuscript editing, R.C.S.; manuscript revision/review, R.C.S., J.A.D., G.F., E.A.; manuscript final version approval, all authors

The purpose of this study was to demonstrate the use of a transrectal system that enables precise magnetic resonance (MR) image guidance and monitoring of prostate interventions. The system used a closed-bore 1.5-T MR imaging unit and enables one to take advantage of the higher signal-to-noise ratio achieved with traditional magnet designs, which is crucial for accurate targeting and monitoring of prostate interventions. In the first of the four canine studies, reliable needle placement, with all needles placed within 2 mm of the desired target site, was achieved. In two other studies, MR imaging was used to monitor distribution of injected contrast agent solution (gadopentetate dimeglumine mixed with trypan blue dye) in and around the prostate, thereby confirming that solution had been delivered to the desired tissue and also detecting faulty injections. In the final study, accurate placement and MR imaging of brachytherapy seeds in the prostate were demonstrated. The described system provides a flexible platform for a variety of minimally invasive MR image–guided therapeutic and diagnostic prostate interventions.

Prostate carcinoma is the most commonly diagnosed life-threatening cancer in men in the United States. In 2002, the estimated incidence of this disease in male patients in the United States was 189,000 (1). As the incidence of prostate cancer is known to increase with age, this cancer will become more common as the U.S. population ages (2). Moreover, due to the widespread acceptance of prostate-specific antigen screening, routine rectal examination, and transrectal ultrasonographic (US) image–guided prostate biopsy, there has been a great increase in the early detection of prostate cancer (3).

Despite this early detection, the appropriate clinical management of prostate cancer is a very controversial subject. There is serious debate regarding the clinical relevance of low-grade prostate cancer. In some cases, prostate cancers grow very slowly and never become clinically important, whereas in other cases, these cancers are very aggressive and dangerous. Because foci of prostate cancer have been incidentally discovered at autopsy in more than 30% of men older than 50 years, it is clear that aggressive treatment is not always appropriate for this malignancy (4,5). Nevertheless, reports (6–8) have shown that overly conservative management (ie, "watchful waiting") can result in poor patient outcomes. Clinical decision making is further complicated by the fact that most prostate cancers are assessed at diagnosis as "intermediate stage" and therefore carry an uncertain prognosis (9).

Currently, the two most accepted methods for treatment of localized prostate cancer are radical prostatectomy and radiation therapy (10). Although both of these approaches are associated with a good chance of a cure, they are also associated with a substantial risk of morbidity, including incontinence, rectal toxicity, and erectile dysfunction (11). Owing to these conflicting factors, there have been increased efforts to develop focal minimally invasive treatment modalities that can be used to target cancerous tissue while reducing morbidity and treatment duration (12).

Effective image guidance of these minimally invasive therapies requires *(a)* excellent visualization of the prostate and the surrounding anatomy so that cancerous tissue can be treated while nearby neural and vascular structures are avoided and *(b)* visualization of the therapeutic agent itself for direct confirmation that the desired abnormal tissue has been treated. On

the basis of these conditions, magnetic resonance (MR) imaging is the best modality for image guidance because it yields excellent soft-tissue contrast, has multiplanar capabilities, and has the potential to yield spectral and biologic information (13). MR imaging has been shown to enable far better visualization of the prostate and surrounding structures than either US or computed tomography (14). Moreover, with MR imaging it is possible to visualize injected liquid agents (15,16), solid implanted therapeutic seeds (eg, brachytherapy seeds) (14,17), and thermal therapy (by means of both direct temperature monitoring and imaging of tissue damage) (18,19). We emphasize that the ability to visualize the therapeutic agent is very enabling in that it allows direct positive confirmation of treatment delivery.

The purpose of our study was to demonstrate the use of a transrectal system that enables precise guidance and monitoring of prostate interventions with a 1.5-T MR imaging unit.

Materials and Methods

A mechanically actuated transrectal needle guide is used to perform MR image–guided needle placement in the prostate. With a microcoil tracking method, we are able to quickly (60 msec) and accurately locate the position and orientation of the needle guide in the MR imaging volume. Knowing the position of the needle enables acquisition of real-time MR images of an anatomic plane containing the needle path and determination of the needle position relative to previously acquired high-spatial-resolution images of the prostate.

Device Design

A thin-walled plastic cylindrical sheath (Delrin plastic; Du Pont, Wilmington, Del) with a radius of 1.5 cm is inserted into the rectum to create a stable and stationary entry point through which the prostate can be accessed (Fig 1, *A*). Integral to the sheath is a 2.5-cm-diameter single-turn coil for local imaging of the prostate. A window within the imaging coil in the sheath allows the needle to be advanced from inside the sheath, through the rectal wall, and into the body of the prostate.

Next, a cylindrical needle guide (Fig 1, *B*), which also is made of Delrin plastic, is placed in the rectal sheath (Fig 1, *C*). The needle guide is coaxial to the rectal sheath and thus is free to rotate and translate within the cavity formed by the sheath without causing deformation of the surrounding soft tissue. Integral to the needle guide are three fiducial microcoils and a curved channel for the needle (Fig 1, *D*). Because the needle channel is curved, the needle can be inserted along the axis of the needle guide and emerge from its lateral wall to allow access to the prostate through the window in the stationary rectal sheath.

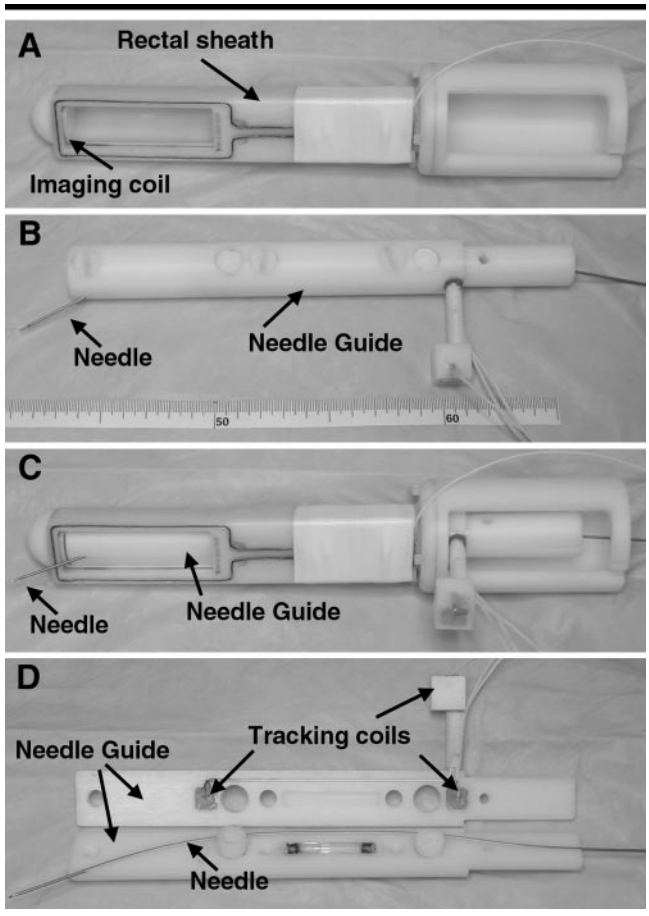

Figure 1. Rectal sheath and needle guide. *A,* A stationary rectal sheath with a radius of 1.5 cm forms a stable access route through which the prostate can be reached. A single-turn rectal imaging coil with tuning, matching, and decoupling elements is included in the sheath. A cylindrical needle guide *(B)* is placed inside the stationary rectal sheath *(C),* allowing rotational and translational degrees of freedom. *D,* The needle guide includes three tracking microcoils and a curved needle channel, which allows access to the prostate laterally through the rectal wall.

Next, both the rectal sheath and the needle guide are affixed to a positioning stage made of nylon and Delrin plastic (Quality Transmission Components, New Hyde Park, NY) (Fig 2, *A*). This positioning stage serves to hold the rectal sheath stationary in the rectum. A linear track (ie, aluminum rail; 80/20, Columbia City, Ind) and a polyamide plastic articulated arm with six joints allow full mobility of the positioning stage so that it can be easily docked with the rectal sheath (Fig 2, *B*). After the stage is docked with the sheath, the linear track and articulated arm are locked down to prevent subsequent motion.

In addition to holding the rectal sheath stationary, the positioning stage contains a screw-drive mechanism that allows both rotation and translation of the needle guide. This device converts the rotation of two concentric control rods (Epoxy Tubing; TAP Plastics, Dublin, Calif), both of which extend outside the magnet bore, into rotation and translation of the needle guide; this process allows the operator to position the needle guide while the subject is in the closed MR magnet bore (Fig 2, *C*).

The entire device was constructed with a coaxial design, so the central axis represents an unobstructed path for insertion of the needle. The depth of needle insertion is controlled by using a variable

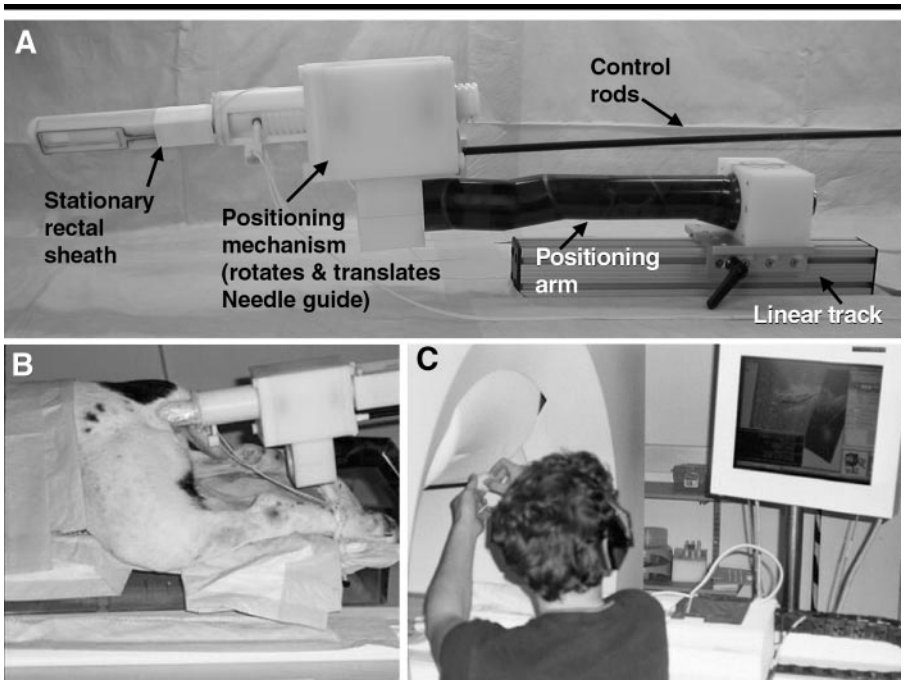

Figure 2. Assembled interventional device. *A,* The stationary rectal sheath and needle guide are affixed to the positioning stage. With use of a flexible articulated arm and a linear track, the device can be positioned freely until both the arm and the track are locked into position. The positioning mechanism converts rotation of the two concentric control rods into rotation and translation of the needle guide within the stationary rectal sheath. *B,* The sheath is positioned inside the rectum and held stationary by the positioning arm and linear track. *C,* By rotating the two control rods located outside the bore, the needle guide can be positioned within the rectum.

offset stop that is inserted at the back of the device before the needle is introduced. An 18-gauge coaxial needle (MRI Devices Daum, Schwerin, Germany) is inserted so that the needle tip will emerge from the side of the needle guide.

Device Tracking, Prostate Targeting, and Real-Time Imaging

The MR pulse sequences and hardware were designed to facilitate targeted needle placement in the prostate within a 1.5-T MR imaging unit (CV/i; GE Medical Systems, Waukesha, Wis) with four independent receiver channels. Three fiducial microcoils, each connected to a separate receiver channel, were integrated within the transrectal needle guide. To determine the position and orientation of these coils, we obtained 12 one-dimensional dodecahedrally spaced MR signal readouts (5.0/2.3 [repetition time msec/echo time msec], bandwidth of ±64 kHz, 1° flip angle, 40-cm field of view, 256 readout points), allowing for coil localization, as described previously (20,21). MR signal acquisition for coil localization took approximately 60 milliseconds. Microcoil localization errors due to gradient nonlinearity were avoided by using gradient dewarping algorithms (GE Medical Systems).

Given the positions of the three fiducial microcoils in the MR imaging coordinate system and the location of a given intraprostatic target (also in the MR imaging coordinate system), the remaining task was to determine *(a)* the degree of rotation and translation necessary to position the needle guide such that the needle trajectory would be aligned with the target and *(b)* the depth of needle insertion necessary to reach the target. These parameters can be calculated by using a set of coordinate transformations, with the assumption that all relationships among the microcoil positions, device axis, and needle trajectory are known. These relationships were established by using a device-calibration MR image set on which gadopentetate dimeglumine–enhanced (Magnevist; Berlex Laboratories, Wayne, NJ) fiducial tubes defined the device axis and the needle trajectory; this same calibration image set was used for all of the studies described herein.

Calibrating the microcoil positions with the needle trajectory not only allowed for determination of the degree of rotation and translation necessary to reach the target site, but it also allowed us to define the imaging plane that included both the needle path and the device axis. Real-time MR images were acquired on the basis of the position of the fiducial microcoils so that the needle could be visualized as it was being inserted into the prostate.

All experiments were performed by using the CV/i 1.5-T imaging unit. A fast gradient-echo (GRE) pulse sequence was modified to allow alternating acquisition of the microcoil-tracking MR signal readouts (ie, the 12 dodecahedrally spaced readouts) and real-time fast GRE images. After the location of each coil was determined, the position and orientation of the imaging plane were defined such that the real-time fast GRE image section contained the path of the needle.

Real-time data were processed and displayed on a workstation (Sun Ultra II; Sun Microsystems, Mountain View, Calif) that was connected to the imaging unit with a high-bandwidth data bus (SBS Technologies, Carlsbad, Calif). With the described transrectal device, the tracking sequence is currently performed in 60 msec; image processing, communication, and imaging plane localization, in 150 msec; and image acquisition, in 300–1,300 msec. The entire process yields frame rates of 0.7–2.0 frames per second (depending predominantly on the image acquisition time). One receiver channel was used for the endorectal imaging coil, used to acquire images of the prostate, whereas the other three receiver channels were connected to each of the three fiducial microcoils.

Animal Study Protocol

All animal study protocols were reviewed and approved by the Johns Hopkins University animal care and use committee. A technician anesthetized four mongrel dogs that weighed approximately 25 kg by means of a bolus injection of thiopental; anesthesia was maintained with 1% isoflurane throughout the experiment. An intravenous catheter was placed in the right jugular vein for fluid administration, and a Foley catheter was inserted to help stabilize the prostate and define the position of the prostatic urethra. The animals were placed in a prone position on the MR imaging table with the pelvis slightly elevated (approximately 10 cm), and a 5-inch surface coil was placed on the anterior surface of the abdomen at the level of the prostate. The rectal sheath was inserted into the rectum and docked with the positioning stage, which was then locked in place. All

experiments were performed by four authors (R.C.S., A.K., G.F., E.A.).

Needle Placement

In the first animal study, the accuracy of needle placement was tested in vivo. One canine was positioned in the MR imaging unit, and then T1-weighted fast spin-echo (SE) images (700/9.2, bandwidth of ±31.25 kHz, echo train length of four, 16-cm field of view, 3-mm section thickness, 0.5-mm intersection spacing, 256 × 256 matrix, four signals acquired, imaging time of 3 minutes) of the prostate and surrounding anatomy were acquired. Two receiver channels were used to acquire these images: one for the 5-inch surface coil and one for the rectal coil. A target in the body of the prostate was selected on these images and entered into the real-time control program. We then changed to the real-time fast GRE (5.1/2.3, bandwidth of ±64 kHz, 10° flip angle, 32-cm field of view, 1-cm section thickness, 256 × 128 matrix, imaging time of 0.65 second) imaging and tracking sequence.

While performing the real-time fast GRE MR imaging and tracking sequence, the operator is able to rotate and translate the needle guide from outside of the magnet bore by rotating the two coaxial control rods. On a flat-panel display screen in the room with the MR imaging unit, the operator views both the real-time image section that depicts the trajectory of the needle and the numeric values that indicate the current degree of rotation and translation necessary to set the correct needle trajectory. As the needle guide is moved closer to the target area, these numbers move toward zero, which indicates that no more rotation or translation is necessary.

Once the needle guide is on the proper trajectory, the insertion stop is set to the proper depth (also indicated on the flat-panel display screen), and the needle is pushed until its handle is flush with the stop (Fig 3, *A*). The insertion of the needle is visualized on the imaging room display screen, and once the needle is in place, the needle tip is at the desired target location.

To confirm the location of the needle tip, we acquired a second set of T1-weighted fast SE MR images. These SE MR images were used to minimize needle susceptibility artifacts (by minimizing T2* effects) and therefore maximize the accuracy in locating the needle tip. The location of the needle tip artifact relative to the selected target point was compared by two authors (R.C.S., E.A.). This protocol was repeated for four separate needle insertions.

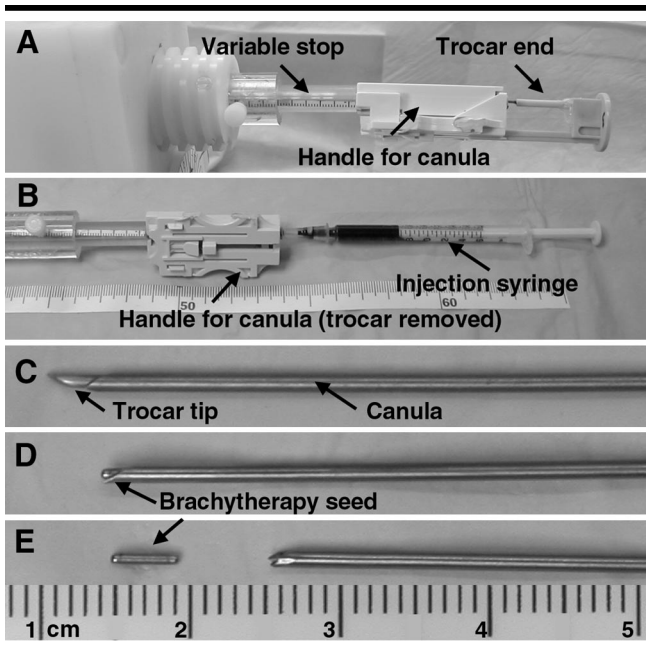

Figure 3. Needle insertion and therapy delivery. *A,* A variable stop is used to control the depth of needle insertion. *B,* After the trocar (ie, inner stylus) is removed, the cannula remains as a hollow conduit through which fluid can be injected into the prostate. *C,* To place brachytherapy seeds, the trocar and cannula are first advanced together. *D,* Then, after the trocar is withdrawn, a brachytherapy seed is pushed to the end of the cannula with a second trocar. *E,* With the trocar held stationary, the cannula is withdrawn, ejecting the seed into the tissue. The trocar and cannula are then withdrawn together.

Intraprostatic Injection

To demonstrate MR image–based monitoring of injected therapies, intraprostatic injections were performed in two canines. Similar to targets in the needle placement study, targets for intraprostatic injection were selected on transverse T1-weighted fast SE MR images, and the needle tip was placed at these locations by using the real-time fast GRE MR imaging and tracking sequence. After the coaxial needle was placed, the trocar (ie, an inner stylus) was withdrawn, leaving only the 18-gauge cannula (ie, a hollow metal tube) in place. This process created a conduit through which injections into the body of the prostate could be performed (Fig 3, *B*).

In this experiment, 0.3 mL of a mixture of 0.4% trypan blue dye (Sigma-Aldrich, St Louis, Mo) and 30 mmol/L gadopentetate dimeglumine was injected into the prostate. During the injection, the flow of the mixture was monitored by using a high-flip-angle radiofrequency-spoiled fast GRE MR imaging sequence (6/1.5, 90° flip angle, bandwidth of ±62.5 kHz, 16-cm field of view, 10-mm section thickness, 256 × 160 matrix, acquisition time of 0.96 second per image). The location of the injected solution was determined by comparing the transverse fast spoiled GRE MR images (80/2.0, 60° flip angle, bandwidth of ±31.25 kHz, 16-cm field of view, 3-mm section thickness, 0.5-mm intersection spacing, 256 × 256 matrix, four signals acquired, imaging time of 1 minute 20 seconds) acquired before with those acquired after the injection. Immediately following the injection procedures and the sacrificing of the animals, the canine prostates were removed, fixed in formalin for 24 hours, sliced into 3-mm axial sections, and then photographed and paired with the corresponding MR image sections by two authors (R.C.S., E.A.).

Brachytherapy Seed Placement

In a fourth canine, the use of the transrectal device for MR image–guided brachytherapy seed placement was demonstrated. Targets were selected, and the trocar and cannula were placed (Fig 3, *C*), as previously described herein. Then, to insert the titanium brachytherapy seeds (OncoSeed Blanks; Medi-Physics, Arling-

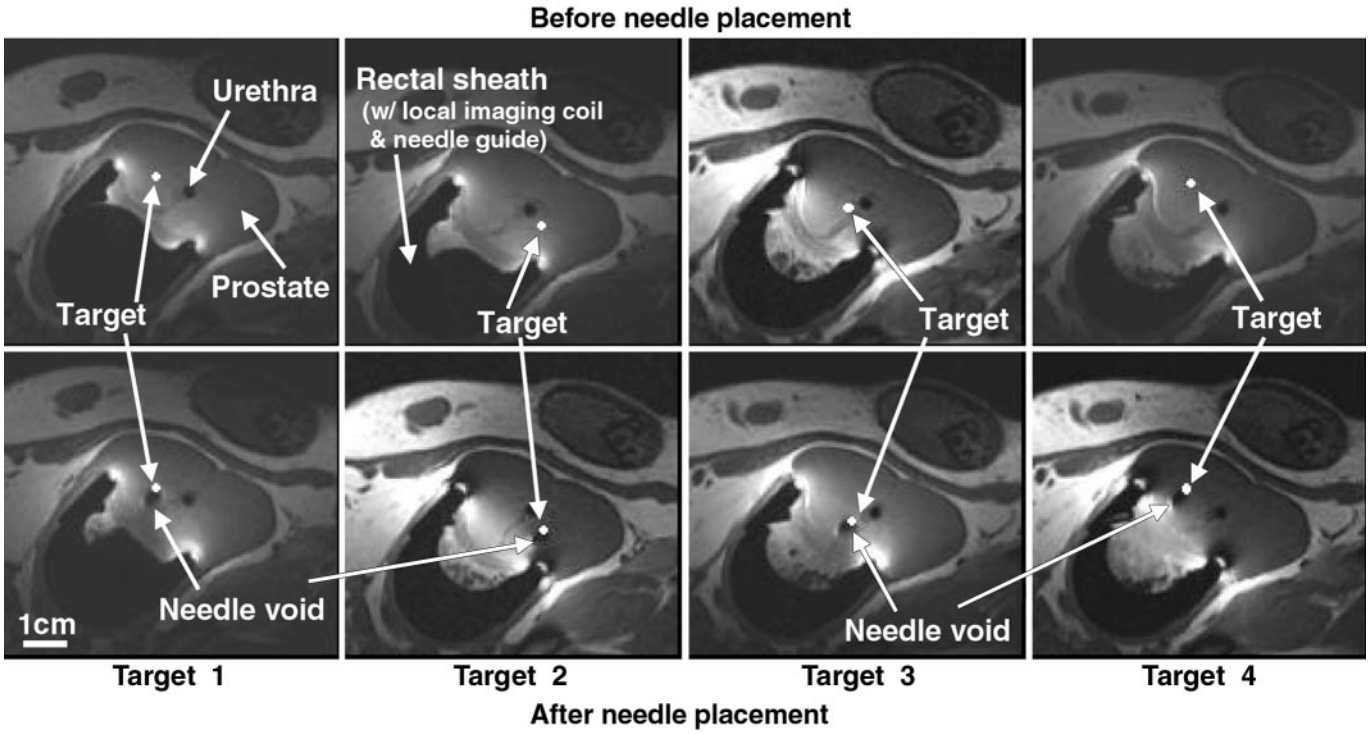

Figure 4. Accurate placement of needles in the canine prostate with use of the transrectal needle guide and microcoil tracking. Top: Four target points in an anesthetized canine were selected on transverse T1-weighted fast SE MR images (700/9.2, bandwidth of ±31.25 kHz, echo train length of four, 16-cm field of view, 3-mm section thickness, 0.5-mm intersection spacing, 256 × 256 matrix, four signals acquired, imaging time of 3 mimutes). Bottom: Transverse T1-weighted fast SE MR images were obtained again after needle placement. The needle tip artifact and the target were found on the same image section, with an in-plane separation of less than 2 mm. Also note that there was minimal motion of the prostate upon needle insertion.

ton Heights, Ill), the trocar was withdrawn, leaving the hollow cannula in place in the prostate. We inserted a brachytherapy seed into the cannula and then advanced it to the end, but not out, of the cannula by pushing it with another trocar (Fig 3, *D*). With the seed at the end of the cannula, we withdrew the cannula slightly while holding the trocar stationary and thus caused the brachytherapy seed to be ejected into the prostate tissue. Subsequently, the trocar and cannula were both withdrawn together (Fig 3, *E*). Three seeds were placed by using this technique. The locations of the needle and the seeds were confirmed by using the same T1-weighted fast SE MR imaging sequence that was used in the needle placement experiments. The MR images were evaluated by two authors (R.C.S., E.A.).

Results

Needle Placement

In the first canine, accurate needle placement in the body of the prostate was achieved. The results of this experiment are summarized in Figure 4. In sequential order, four targets were selected on T1-weighted fast SE images (Fig 4, top row). Having placed the needle by using the fast GRE real-time MR imaging and tracking sequence, we performed fast SE MR imaging again to confirm the placement of the needle by visualizing the needle void (Fig 4, bottom row). In all cases, both the end of the needle artifact and the target were visualized on the same image section (section thickness, 3 mm). Moreover, the center of the needle tip void was found within 2 mm (in-plane) of the selected target. Note also that there was minimal motion of the prostate due to insertion of the needle.

To interpret the results of the needle placement study, it is necessary to examine the artifact created by the 18-gauge MR imaging–compatible needle. Figure 5 shows the artifacts created by the needle and a brachytherapy seed. We aligned the artifacts by placing the physical objects (ie, needle and brachytherapy seed) at the interface of gadopentetate dimeglumine–doped and gadolinium-free gel blocks. Note that the tip void is a circular bloom centered at the end of the actual needle, as has been previously described when the needle is aligned approximately parallel to the static magnetic field, or B_0, with the tip toward the positive magnet pole (22). In all cases, because of the design of the needle placement system, the needle was approximately parallel to the static magnetic field; therefore, the artifact position is a good estimate of the needle tip position.

Because visual confirmation is not possible in vivo, it was difficult to precisely quantify the accuracy of in vivo needle placement. However, in all in vivo experiments, the needle tip was seen on the same MR imaging section as the target (section, 3 mm) and in-plane needle position errors were less than 2 mm.

Intraprostatic Injection

In two canines, the usefulness of this system for MR image–monitored intraprostatic injections was demonstrated. The box on the sagittal scout MR image (left image) in Figure 6 indicates the location of the time-series MR images acquired during the injection of the gadopentetate dimeglumine–trypan blue dye solution. Note that all of the injected solution remained in the prostate. Therefore, it was confirmed—during the injec-

tion procedure—that the full desired dose was delivered to the prostatic tissue.

In Figure 7, the distribution of the contrast agent–dye solution in the prostate of one canine, as depicted on MR images, is compared with the distribution of the solution seen in the gross tissue slices. There is good agreement between the gadolinium-enhanced tissue depicted on the MR images (Fig 7, second column) and the gross tissue slices stained with trypan blue dye (Fig 7, third column).

The intraprostatic injection experiment was repeated in another canine. In this case, however, the MR images showed the injected contrast agent–dye solution leaking out of the prostate and into the surrounding connective tissue (Fig 8). Therefore, it was known—during the injection procedure—that the desired dose was not delivered to the prostate. In Figure 9, the presence of trypan blue dye in the connective tissue at the superior margin of the prostate is confirmed in the gross tissue slices.

Brachytherapy Seed Placement

In the last canine, the application of this system for brachytherapy seed placement in the prostate was demonstrated. Figure 10, *A* shows the selected targets on coronal MR images of the prostate. Figure 10, *B* shows MR images obtained in the same plane after needle placement. Unlike in the needle placement study, in this experiment, the tip of the needle artifact was seen extending beyond the target point. This is because the brachytherapy seeds were placed at the end of the cannula rather than at the end of the trocar, which extended 2 mm past the end of the cannula. Therefore, for proper seed deposition, the trocar must extend 2 mm past the target point.

Figure 10, *C* shows the seeds placed in the prostate after the coaxial needle had been removed. To interpret these findings, it is helpful to refer to Figure 5, which shows the artifact pattern created by the brachytherapy seeds. In Figure 5, the main signal void is seen at the end of the 4-mm seed that lies nearest to the positive pole of the static magnetic field. This signal void corresponds to the signal void seen in Figure 10, *C*. The bodies of the brachytherapy seeds extend 4 mm from this void in the inferior direction (ie, in the direction of the target location). The seeds lie within 3 mm of the selected target location. Also note that intraprostatic bleeding (ie, the dark banding radiating toward the edge of the prostate) resulting from seed placement can be seen near seeds 2 and 3.

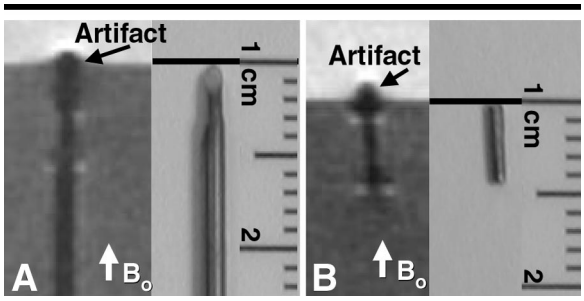

Figure 5. Coronal fast SE MR images (700/9.2, bandwidth of ±31.25 kHz, echo train length of four, 8-cm field of view, 1.5-mm section thickness, 256 × 256 matrix, four signals acquired, imaging time of 3 minutes) obtained in a gel phantom show artifacts created by *A,* the prostate needle and *B,* the brachytherapy seed. Both objects created a uniform signal void along their lengths and a circular bloom, centered on the object tip, at the end facing the positive pole of the static magnetic field. The labeled arrow *(B_0)* denotes the positive direction of the static magnetic field. The artifacts were aligned by placing the physical objects (ie, needle and seed) at the interface of gadopentetate dimeglumine–doped and gadolinium-free gel blocks.

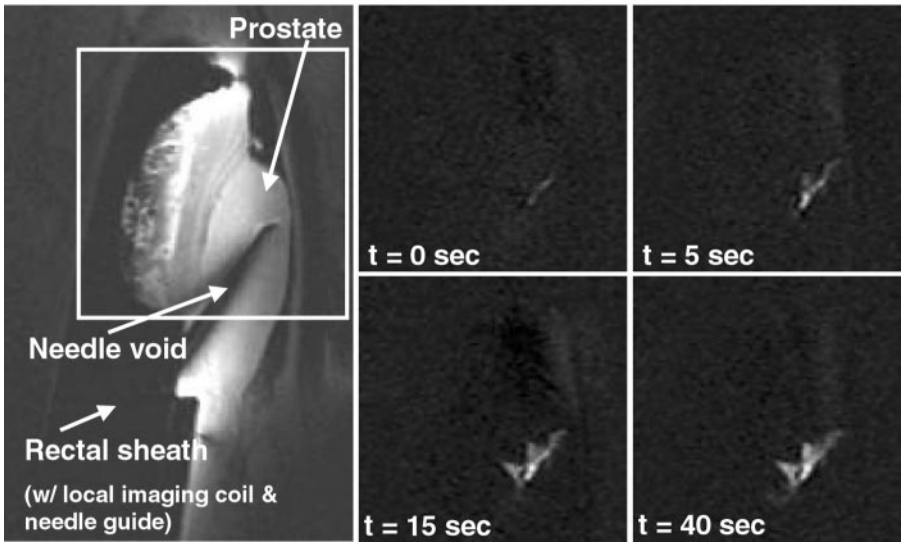

Figure 6. Intraprostatic injections of a solution consisting of 0.4% trypan blue dye and 30 mmol/L of gadopentetate dimeglumine depicted on fast spoiled GRE MR images. The box on the sagittal scout MR image (left) indicates the location of the time-series images (6/1.5, 90° flip angle, bandwidth of ±62.5 kHz, 16-cm field of view, 10-mm section thickness, 256 × 160 matrix, acquisition time of 0.96 second per image). Note that all of the injected contrast agent–dye solution remained in the canine prostate. Therefore, it was confirmed that the full desired dose was delivered to the tissue. *t* = elapsed time between the beginning of contrast agent administration and the image acquisition.

Discussion

Our study results show that needles can be accurately placed in the body of the prostate gland while the subject is in a closed-bore 1.5-T MR imaging unit. Although diagnostic biopsy was not a focus of the current study, it is an obvious subsequent application. Currently, transrectal US–guided needle biopsy is the reference standard for the diagnosis of prostate cancer (23). Although this method has excellent specificity, it is not very sensitive. Transrectal US–guided biopsy does not detect the presence of prostate cancer in approximately 20% of cases (24). MR imaging, in contrast, has high sensitivity for detection of prostate tumors (25). MR imaging alone without concurrent biopsy, however, has low diagnostic specificity.

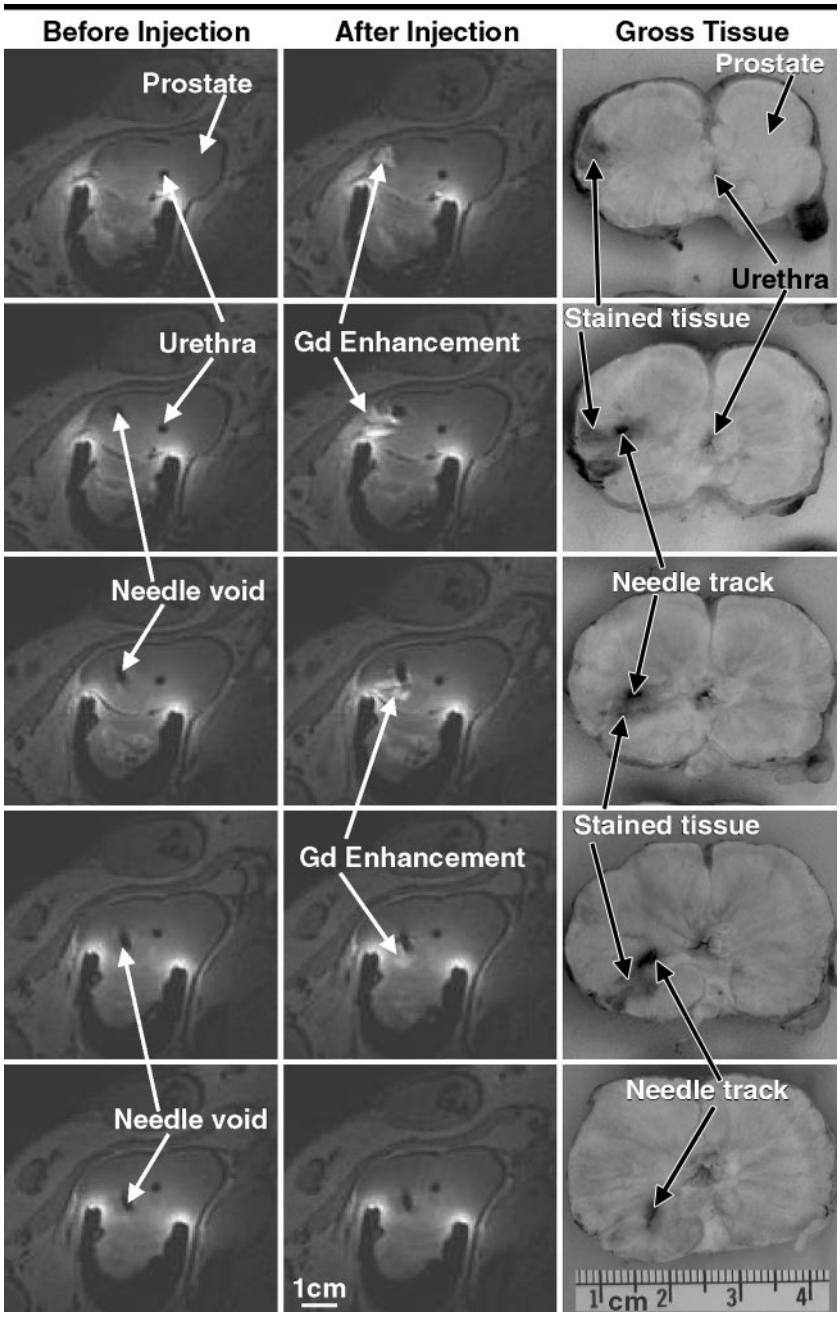

Figure 7. Distribution of injected contrast agent–dye solution depicted on transverse fast spoiled GRE MR images (80/2.0, 60° flip angle, bandwidth of ±31.25 kHz, 16-cm field of view, 3-mm section thickness, 0.5-mm intersection spacing, 256 × 256 matrix, four signals acquired, imaging time of 1 minute 20 seconds) and confirmed in gross tissue slices. The distribution of the gadolinium–blue dye solution as visualized with MR imaging (enhancement seen in postinjection but not preinjection MR images) matches with the distribution of blue-stained tissue seen in the gross tissue slices.

To take advantage of the high diagnostic sensitivity of MR imaging while maintaining the specificity of biopsy, the described transrectal system may be useful for performing MR image–guided prostate biopsy. Although it would not be practical to perform all prostate biopsies with MR image guidance, the excellent tissue contrast achieved with MR imaging is very useful for targeted tissue biopsy. In men who have consistently increasing prostate-specific antigen levels (indicating a high likelihood of cancer) but repeatedly negative US-guided biopsy findings, MR image–guided biopsy may yield a definitive diagnosis. The usefulness of MR imaging in this application area has been demonstrated in a low-field, open-bore magnet by using a transperineal approach to the prostate (26). The system described here is well suited for image-guided biopsy because it uses a standard transrectal approach to the prostate and a closed-bore MR unit; thus, the higher signal-to-noise ratio that is vital for tumor visualization can be achieved. Moreover, higher field strength creates the potential for targeted biopsy of MR spectroscopically defined prostate lesions and thus improved diagnostic accuracy (13).

Second, MR image–targeted prostate biopsy may have the anatomic accuracy that is necessary for long-term monitoring of prostate lesions. With current US-guided biopsy procedures, it is very difficult to repeatedly collect tissue from the same location in the prostate because of poor anatomic visualization. Given the current increase in the early detection of prostate cancers and the prevalence of intermediate-stage prostate tumors, which are associated with an uncertain prognosis (9), it would be very useful to be able to repeatedly "sample" a tumor over a several-year period. This would allow better clinical decision making—for example, definitive prostatectomy or radiation therapy could be delayed until it was absolutely necessary or possibly indefinitely.

With MR imaging, the distribution of therapeutic agents injected into the prostate can be directly verified. MR imaging enables visualization of not only the tissue itself but also the therapeutic agent. It is therefore possible to verify when the tissue has been treated and, most important, when an injection has been unsuccessful—that is, the injected substance has been delivered into surrounding tissue rather than to the desired target area. With the advent of local targeted treatments for prostate cancer (12,27), it is important to confirm that therapy delivery has been successful. Otherwise, a potentially valuable agent could be labeled as ineffective because it never reached the target site.

In the final study of this work, the usefulness of MR imaging for guiding brachytherapy seed placement was demonstrated. Brachytherapy seeds are commonly placed by using transrectal US guidance while the seeds are inserted through the perineal surface (28). Given the poor soft-tissue contrast achieved with US, however, it is common for the seeds to be misplaced in nearby tissue (29). In a recent study (30), radiation

seeds were found in the lungs of 36% of patients after they had undergone US-guided prostate brachytherapy: Seeds may be inadvertently placed in the venous plexus surrounding the prostate, where they then may travel to the lungs. MR image–guided seed placement would be useful in such cases because it yields good anatomic definition. An MR image–guided seed placement system would be suitable for the placement of a few therapy seeds near a small lesion in the prostate.

Two important aspects of the described system design need to be emphasized. First, the stationary rectal sheath is essential for high-spatial-resolution imaging and the stability of the prostate. The thin-walled sheath maintains access to the prostate and thus enables easy rotation and translation of the needle guide while minimizing motion of the surrounding tissue. Because the rectum is very sensitive to pain caused by pressure but relatively insensitive to sharp pain, the system can help minimize patient discomfort during the positioning of the needle guide. In addition, the prostate, which is highly deformable, stays relatively fixed throughout the entire procedure. Without the stationary sheath, motion of the needle guide would result in substantial deformation of the prostate, which would complicate the targeting procedure.

Second, we wish to emphasize the importance of using the described transrectal system with a closed-bore 1.5-T MR imaging unit. The main advantages of MR imaging are high spatial resolution and excellent soft-tissue contrast. Although a low-field-strength, open-bore unit would simplify the design of the needle guide system, low field strength marginalizes the usefulness of MR imaging. Therefore, a system that can be used with a conventional closed-bore magnet was designed so that high-quality MR imaging of the prostate could be maintained.

In conclusion, we have described a transrectal system that allows for image–based monitoring of prostate therapy in a closed-bore 1.5-T MR imaging unit. Applications include MR image–based monitoring of intraprostatic injections and brachytherapy seed placement. Because the described transrectal system is used with closed-bore MR imaging units, it enables one to take advantage of the higher signal-to-noise ratio achieved with conventional magnet designs. At present, we are investigating injected therapies such as those involving the use of alcohol, chemotherapeutic agents, and genetic agents.

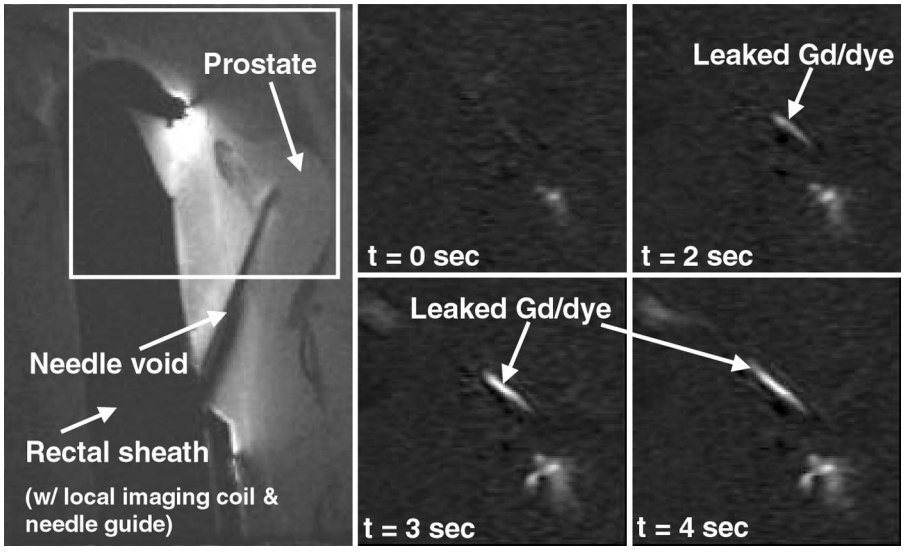

Figure 8. MR image–based monitoring enables detection of faulty injections. The box on the sagittal scout MR image (left) indicates the location of the time-series MR images (6/1.5, 90° flip angle, bandwidth of ±62.5 kHz, 16-cm field of view, 10-mm section thickness, 256 × 160 matrix, acquisition time of 0.96 second per image). In this canine, the injected contrast agent–dye solution leaked out of the prostate and into the surrounding connective tissue. Therefore, it was known—during the procedure—that the desired dose had not been delivered to the prostate. *t* = elapsed time between the beginning of contrast agent administration and the image acquisition.

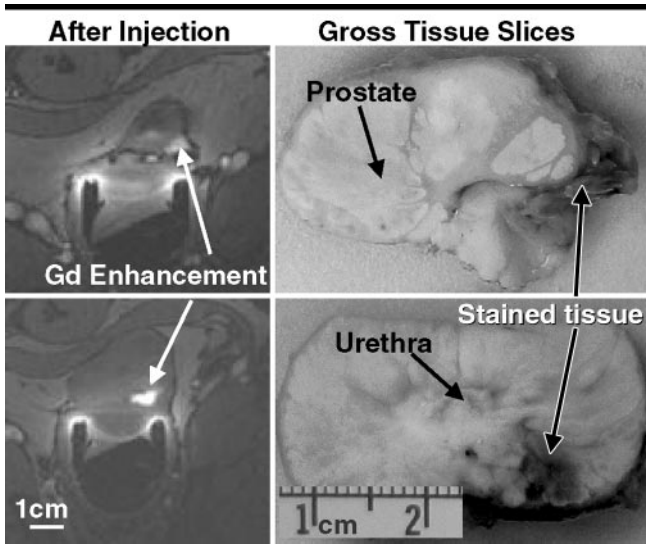

Figure 9. Leakage of injected contrast agent–dye solution into surrounding tissue is confirmed on transverse fast spoiled GRE MR images (80/2.0, 60° flip angle, bandwidth of ±31.25 kHz, 16-cm field of view, 3-mm section thickness, 0.5-mm intersection spacing, 256 × 256 matrix, four signals acquired, imaging time of 1 minute 20 seconds) and in the corresponding gross tissue slices. The distribution of the gadolinium-based solution, seen as an area of high signal intensity (arrows) on the MR images, correlates with the distribution of the solution seen in the stained canine prostate tissue sections. Although some solution remained in the prostate, some solution also passed into the connective tissue at the superior left margin of the posterior region of the prostate.

Acknowledgments: The authors thank Andrew C. H. Yung, MS, for help with the experiments and the endorectal imaging coil design; Jason A. Polzin, PhD, for assistance with the gradient dewarping algorithms; Theodore L. Deweese, MD, for advice regarding clinical applications; and Elliot R. McVeigh, PhD, for providing additional laboratory and imaging resources.

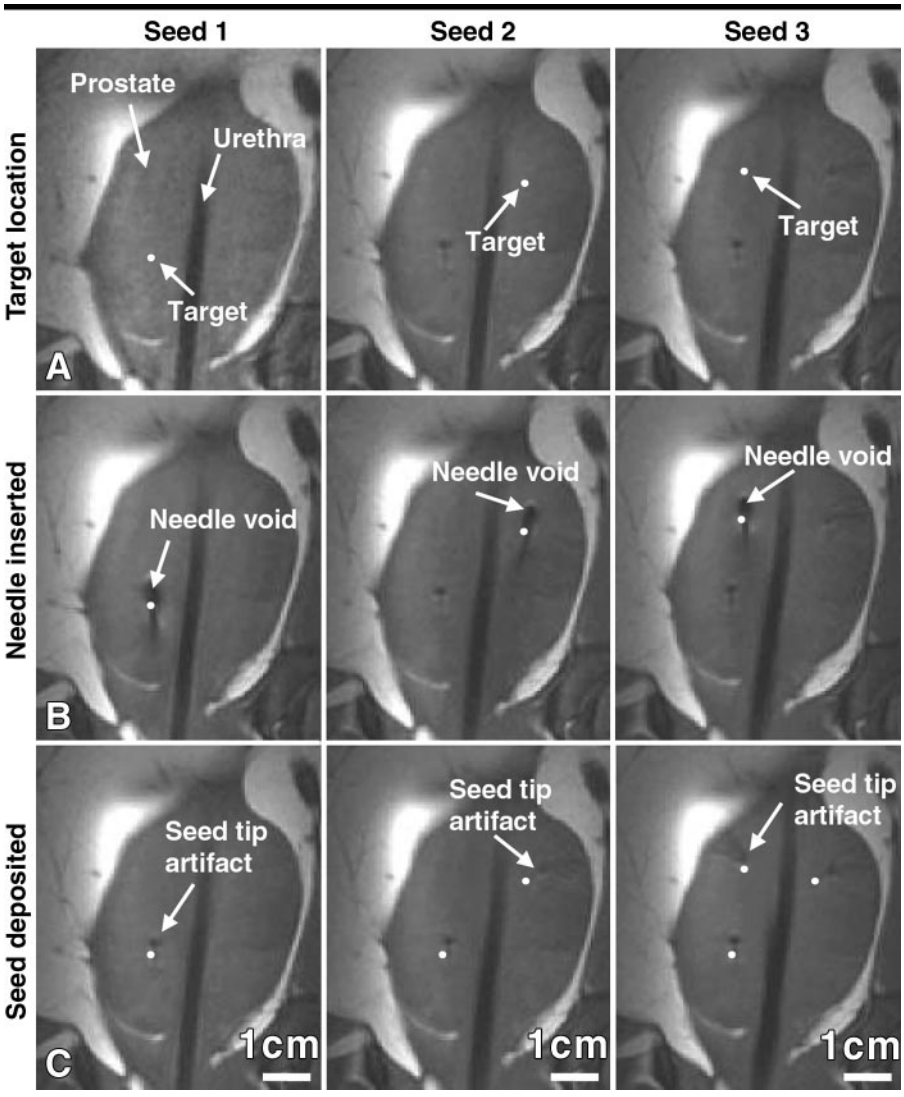

Figure 10. MR image guidance enables accurate placement of brachytherapy seeds in a canine prostate. *A,* Three target areas in one plane of the prostate were selected on coronal fast SE MR images (700/9.2, bandwidth of ±31.25 kHz, echo train length of four, 16-cm field of view, 3-mm section thickness, 0.5-mm intersection spacing, 256 × 256 matrix, four signals acquired, imaging time of 3 minutes). *B,* The needle was placed at these locations as described previously. Because the brachytherapy seeds were placed at the end of the cannula (2 mm back from the end of the trocar tip), the needle artifact extended beyond the target site by approximately 2 mm. In *C,* the seeds have been placed in the prostate. The black bloom artifact at the superior end of the 4-mm brachytherapy seeds is visible. The seeds extended 4 mm from this artifact in the inferior direction.

References

1. Jemal A, Thomas A, Murray T, Thun M. Cancer statistics, 2002. CA Cancer J Clin 2002; 52:23–47.
2. Carter HB, Piantadosi S, Isaacs JT. Clinical evidence for and implications of the multistep development of prostate cancer. J Urol 1990; 143: 742–746.
3. Slawin KM, Ohori M, Dillioglugil O, Scardino PT. Screening for prostate cancer: an analysis of the early experience. CA Cancer J Clin 1995; 45:134–147.
4. Franks LM. Latent carcinoma of the prostate. J Pathol Bact 1954; 68:603–616.
5. Dhom G. Epidemiologic aspects of latent and clinically manifest carcinoma of the prostate. J Cancer Res Clin Oncol 1983; 106:210–218.
6. Brasso K, Friis S, Juel K, Jorgensen T, Iversen P. The need for hospital care of patients with clinically localized prostate cancer managed by noncurative intent: a population based registry study. J Urol 2000; 163:1150–1154.
7. Adolfsson J, Steineck G, Hedlund PO. Deferred treatment of clinically localized low-grade prostate cancer: actual 10-year and projected 15-year follow-up of the Karolinska series. Urology 1997; 50:722–726.
8. Chodak GW, Thisted RA, Gerber GS, et al. Results of conservative management of clinically localized prostate cancer. N Engl J Med 1994; 330: 242–248.
9. Ohori M, Wheeler TM, Scardino PT. The New American Joint Committee on Cancer and International Union Against Cancer TNM classification of prostate cancer: clinicopathologic correlations. Cancer 1994; 74:104–114.
10. Pirtskhalaishvili G, Hrebinko RL, Nelson JB. The treatment of prostate cancer: an overview of current options. Cancer Pract 2001; 9:295–306.
11. Potosky AL, Legler J, Albertsen PC, et al. Health outcomes after prostatectomy or radiotherapy for prostate cancer: results from the Prostate Cancer Outcomes Study. J Natl Cancer Inst 2000; 92:1582–1592.
12. Carroll PR, Presti JC Jr, Small E, Roach M III. Focal therapy for prostate cancer 1996: maximizing outcome. Urology 1997; 49:84–94.
13. Koutcher JA, Zakian K, Hricak H. Magnetic resonance spectroscopic studies of the prostate. Mol Urol 2000; 4:143–152.
14. Yu KK, Hricak H. Imaging prostate cancer. Radiol Clin North Am 2000; 38:59–85.
15. Lederman RJ, Guttman MA, Peters DC, et al. Catheter-based endomyocardial injection with real-time magnetic resonance imaging. Circulation 2002; 105:1282–1284.
16. Yang X, Atalar E, Li D, et al. Magnetic resonance imaging permits in vivo monitoring of catheter-based vascular gene delivery. Circulation 2001; 104:1588–1590.
17. D'Amico AV, Cormack R, Tempany CM, et al. Real-time magnetic resonance image-guided interstitial brachytherapy in the treatment of select patients with clinically localized prostate cancer. Int J Radiat Oncol Biol Phys 1998; 42:507–515.
18. Chen JC, Moriarty JA, Derbyshire JA, et al. Prostate cancer: MR imaging and thermometry during microwave thermal ablation—initial experience. Radiology 2000; 214:290–297.
19. Graham SJ, Stanisz GJ, Kecojevic A, Bronskill MJ, Henkelman RM. Analysis of changes in MR properties of tissues after heat treatment. Magn Reson Med 1999; 42:1061–1071.
20. Dumoulin CL, Souza SP, Darrow RD. Real-time position monitoring of invasive devices using magnetic resonance. Magn Reson Med 1993; 29:411–415.
21. Derbyshire JA, Wright GA, Henkelman RM, Hinks RS. Dynamic scan-plane tracking using MR position monitoring. J Magn Reson Imaging 1998; 8:924–932.
22. Liu H, Martin AJ, Truwit CL. Interventional MRI at high-field (1.5 T): needle artifacts. J Magn Reson Imaging 1998; 8:214–219.
23. Presti JC Jr. Prostate cancer: assessment of risk using digital rectal examination, tumor grade, prostate-specific antigen, and systematic biopsy. Radiol Clin North Am 2000; 38:49–58.
24. Keetch DW, Catalona WJ, Smith DS. Serial prostatic biopsies in men with persistently elevated serum prostate specific antigen values. J Urol 1994; 151:1571–1574.
25. Wefer AE, Hricak H, Vigneron DB, et al. Sextant localization of prostate cancer: comparison of sextant biopsy, magnetic resonance imaging and magnetic resonance spectroscopic imaging with step section histology. J Urol 2000; 164:400–404.
26. Hata N, Jinzaki M, Kacher D, et al. MR imaging-guided prostate biopsy with surgical navigation software: device validation and feasibility. Radiology 2001; 220:263–268.
27. DeWeese TL, van der Poel H, Li S, et al. A phase I trial of CV706, a replication-competent, PSA selective oncolytic adenovirus, for the treatment of locally recurrent prostate cancer following radiation therapy. Cancer Res 2001; 61: 7464–7472.
28. Ragde H, Grado GL, Nadir B, Elgamal AA. Modern prostate brachytherapy. CA Cancer J Clin 2000; 50:380–393.
29. Coakley FV, Hricak H. Radiologic anatomy of the prostate gland: a clinical approach. Radiol Clin North Am 2000; 38:15–30.
30. Ankem MK, DeCarvalho VS, Harangozo AM, et al. Implications of radioactive seed migration to the lungs after prostate brachytherapy. Urology 2002; 59:555–559.